Fringe pattern inpainting based on dual-exposure fused fringe guiding CNN denoiser prior

Peng Guangze, Chen Wenjing*

Department of Optic-Electronic, College of Electronics and Information Engineering,
Sichuan University, Chengdu, Sichuan 610065, China

*Corresponding author: chenwj0409@scu.edu.cn

The intensity of some pixels of the captured fringe will be saturated when fringe projection pro-filometry is used to measure objects with high reflectivity, which will significantly affect the re-construction of the measured object. In this paper, we propose a fringe pattern inpainting method based on the convolutional neural network (CNN) denoiser prior guided by additional information from a fringe captured in short exposure time. First, a binary mask obtained by Otsu algorithm from the modulation information of the short exposure fringe is used to detect the high-saturation region in the normal exposure fringe. Then, the corrected gray-scales of the region of the short exposure fringe selected by the mask are inserted in the saturated region of the normal fringe to form an initial fringe for iteration. At last, fringe pattern inpainting is achieved by using a CNN denoiser prior. The correct phase can be reconstructed from the inpainted fringes. The computer simulation and experiments verify the effectiveness of the proposed method.

Keywords: fringe projection profilometry, phase calculation, convolutional neural network, denoiser prior.

1. Introduction

Fringe projection profilometry (FPP) is a widely used active optical three-dimen-sional (3D) measuring technique. It has the advantages of full-field, high precision and high speed [1, 2]. However, when objects with high dynamic range reflectivity are measured, such as metal parts and china products, some intensity saturation regions will appear in the collected fringe pattern(s) due to the inhomogeneous reflection, which eventually leads to errors in the 3D reconstruction.

Some methods have been proposed to overcome the intensity saturation problem. For instance, according to the polarization characteristic of the reflected light, Salahieh *et al*. [3] eliminated the saturated points by adding a polarizer and selecting a proper angle of polarization; or as Zhang [4] has done, multiple fringe patterns captured in different exposure times were fused to form a high-quality fringe by selecting the pixel with the unsaturated highest intensity from homonymous points of the images; or as references [5, 6] have done, the projecting intensity of the projector was changed to guarantee the high quality in the regions with over low or over high reflectivity.

These methods mentioned above require either complex operational process or additional hardware devices. Some scholars used the image processing technique to directly inpaint the fringe with saturation areas for avoiding time consuming and simplifying the measurement system. BUDIANTO and LUN [7] proposed an iterative regularization inpainting method based on a double tree complex wavelet transform. In reference [8], they demonstrated the importance of the election of an initial iteration fringe and calculated the initial fringe to guide inpainting of the saturated region according to the geometric morphology of the neighborhood stripes. These works inspired us to inpaint fringes by combining the multi-exposure technique and image processing technique.

In this paper, a fringe inpainting method based on a CNN denoiser prior is proposed. As we know, when the surface reflection is mostly considered as the diffuse reflection in imaging process, the intensity of the image can be changed through adjusting the exposure time [9]. The captured fringe pattern in short exposure time can provide the information which has been lost in the saturated region of the normal exposure fringe pattern. The saturated region of the normal exposure fringe pattern is determined by a binary mask obtained by the Otsu method applied on the modulation of the short exposure fringe. The region without fringe is filled up with the corresponding information provided by the corrected gray of the short exposure fringe. The dual-exposure fused fringe provides a suitable initial iterative value for the CNN denoiser to produce a good quality fringe. The inpainted fringe can be used to calculate the correct phase information. Simulations and experiments verify the effectiveness of the proposed method.

2. Basic principles

2.1. Principles of the structured light projection profilometry

Fourier transform profilometry (FTP) [11] and phase-shifting profilometry (PSP) [12] are quite commonly used in the 3D reconstruction. Without loosing generality, in the FTP and PMP, fringe patterns captured by a CCD camera can be expressed as follows:

$$I_i(x, y) = a(x, y) + b(x, y) \cos\left(2\pi f_0 x + \varphi(x, y) + \frac{1}{N} 2\pi i\right) \tag{1}$$

where $I_i(x, y)$ is the intensity of the i-th frame of fringes, $a(x, y)$ is the intensity of background; $b(x, y)$ is the contrast; $\varphi(x, y)$ is the phase information; f_0 is the carrier frequency; N is the number of phase-shifting steps, and $i = 0, 1, 2, \ldots, N-1$.

Phase-shifting profilometry utilizes a phase-shifting algorithm to calculate the phase. Taking the four steps phase-shifting algorithm as an example, the wrapped phase can be expressed as:

$$\varphi(x, y) = \arctan \frac{I_4(x, y) - I_2(x, y)}{I_1(x, y) - I_3(x, y)} \tag{2}$$

The modulation which reflects the reliability of the phase calculation can be regarded as an evaluation parameter of the fringe quality. The modulation information can be calculated by the following formula for the phase-shifting profilometry [13]:

$$M(x, y) = \sqrt{\left[\sum_{i=0}^{N-1} I_i(x, y) \sin\left(\frac{1}{N} 2i\pi\right)\right]^2 + \left[\sum_{i=0}^{N-1} I_i(x, y) \cos\left(\frac{1}{N} 2i\pi\right)\right]^2} \qquad (3)$$

and $N \geq 3$.

In FTP, the Fourier transform spectrum of the fringe is expressed:

$$F(u, v) = F_0(u, v) + F_1(u - f_0, v) + F_{-1}^*(u + f_0, v) \qquad (4)$$

Here $F_0(u, v)$, $F_1(u - f_0, v)$, and $F_{-1}^*(u + f_0, v)$ are the zero order frequency spectrum, the positive first order spectrum and the negative first order frequency spectrum, respectively. The complex signal corresponding to the positive first-order spectrum is calculated by the inverse Fourier transform, which is expressed as:

$$M(x, y) = \frac{1}{2} b(x, y) \exp(2i\pi f_0 x + \varphi(x, y)) \qquad (5)$$

where $b(x, y)/2$ represents the modulation of the fringe pattern, the wrapped phase is embedded in the complex angle. Both in the FTP or PMP method, a phase unwrapping algorithm is needed to obtain the continuous phase. In our work, we utilize the modulation information of fringe pattern(s) to determine saturated regions.

2.2. Image inpainting based on CNN denoiser prior

Image inpainting is a sub-problem of the image restoration (IR). It is aimed to rebuild the missing part of an image. A general model of the image degradation can be expressed as $y = Ax + n$. Here y is the degraded image, x is the original image, n is the noise component, and A is the degradation matrix. From the degraded image y, the optimal solution of the estimated value of the latent ideal image x can be expressed as [14]:

$$\hat{x} = \operatorname*{argmin}_x \frac{1}{2} \|y - A\|^2 + \lambda R(x) \qquad (6)$$

where, $\|y - A\|^2/2$ and $R(x)$ are the fidelity term and the regularization term, respectively. The first term guarantees that the estimated solution conforms to the actual degradation process, and the second term provides effective information about the iterative process. The parameter λ controls the weight of the regularization term in each iterative process.

The most popular methods used to solve Eq. (6) are the model optimization method and the discrimination learning method [15]. The model optimization method can deal with many kinds of image degradation problems by utilizing different degradation ma-

trices. Yet, the discrimination learning method requires a time-consuming training process and it is usually restricted to specialized tasks. But after being trained, the learning-based method can enjoy better time efficiency and tend to have a better performance.

In recent years, more and more attention has been paid to the combination of the two methods. The fusion of the optimization method and the learning-based method normally converts the optimization problem to two individual sub-problems utilizing the variable splitting techniques, such as half quadratic splitting (HQS) [14, 16] method or alternating direction method of multipliers (ADMM) [17]. Solving $\hat{x}$ has been divided into two subproblems: solving the fidelity term and solving the regularization term, respectively. Solving the regularization term is regarded as the image denoising subproblem. Sparse representation [18], block-matching and 3D filtering (BM3D) [19] and the convolutional neural network [20] are the common denoising algorithms. To the best of our knowledge, among all these methods, a well-trained CNN is one of the most powerful denoisers. The application of CNN denoiser in the image inpainting not only retains the flexibility of the model optimization method, but also improves the performance and time efficiency of the learning-based method. Therefore, in our work, a fringe inpainting method using a trained CNN denoiser prior is discussed. Because solving $\hat{x}$ in Eq. (6) has been converted to the iterative denoising problem, a well-pre-trained CNN denoiser is adopted in our work to improve the effect of the fringe inpainting without additional model training and large database acquisition.

In the HQS method, an auxiliary variable z is introduced for solving Eq. (6). The original IR problem described by Eq. (6) can be converted to:

$$L_\mu(x, z) \; = \; \frac{1}{2}\|y - Ax\|^2 + \lambda R(z) + \frac{\mu}{2}\|z - x\|^2 \tag{7}$$

Here, μ is the penalty parameter in the iterative process, k means the number of iterations. Solving Eq. (7) can be replaced by alternately solving the following two subproblems:

$$x_{k+1} \; = \; \arg\min_x \|y - Ax\|^2 + \mu\|x - z_k\|^2 \tag{8a}$$

$$z_{k+1} \; = \; \arg\min_x \frac{\mu}{2}\|z - x_{k+1}\|^2 + \lambda R(z) \tag{8b}$$

Equation (8a) is a constrained least squares problem, which can be solved by the following formula, where I is the identity matrix:

$$x_{k+1} \; = \; (A^\mathrm{T}A + \mu I)^{-1}(A^\mathrm{T}y + \mu z_k) \tag{9}$$

Solving Eq. (8b) is reduced to the Gaussian denoising problem, where λ/μ is the variance of Gaussian noise:

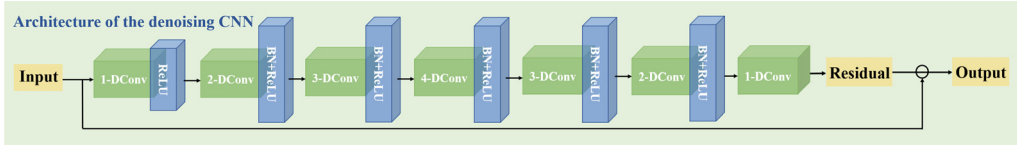$$z_{k+1} \; = \; \mathrm{denoiser}(x_{k+1}\sqrt{\lambda/\mu}) \tag{10}$$

Fig. 1. Architecture of the denoising CNN.

Due to highly parallel characteristic of the CNN, solving Eq. (10) was completed on GPU in our simulation and experiments. Figure 1 is the architecture of the denoising convolution neural network [12]. The designed architecture starts with a convolutional layer and a rectified linear unit (ReLU), followed by five repeated modules sequentially, and ends with convolution layers. Each module consists of a convolutional layer, batch normalization and ReLU. There are 64 convolution kernels in every convolution layer, and each layer uses dilated convolution with parameters of 1, 2, 3, 4, 3, 2, 1, respectively.

3. Inpainting the saturated region of fringe pattern

An additionally captured short exposure fringe is used to fill up the saturated region in the normal exposure fringe to form an initial iterative fringe as one of the inputs of the CNN denoiser to inpaint the fringe. The complete inpainting process is listed as following: 1) Two fringes are captured in exposure time T and T', respectively. In our experiment, T' was set to be about one-thirtieth of T. In fact, the short exposure time is determined on the premise that the fringe quality in the region corresponding to the saturated region of the normal exposure fringe is satisfying. 2) The Otsu method is used to determine the saturated region from the modulation of the short exposure fringe. 3) The initial iterative fringe used in the fringe inpainting is determined by fusing two fringes with different exposure times. 4) Fringe inpainting is achieved by using CNN denoiser prior quickly. Some details will be given in the following parts.

3.1. Saturated region detection

The modulation information on fringe is used to determine the saturated region. As we all know, the modulation in the saturated region is low. It is difficult to select the saturated region from the other region with low modulation values in the normal exposure fringe. Therefore, the modulation map of the short exposure fringe is selected to detect the saturation area. Although the short exposure fringe pattern avoids the appearance of the saturation area, the contrast and the signal to noise ratio (SNR) of the fringes are unavoidably low. In order to suppress the effect of noise component, the Fourier transform method is selected to calculate the modulation of the short exposure fringe. Figure 2 shows a comparison result of the saturated regions determined from the modulation images obtained from the normal exposure fringe and the short exposure fringe, respectively. Figures 2**a** and 2**d** are the fringes captured in the normal and
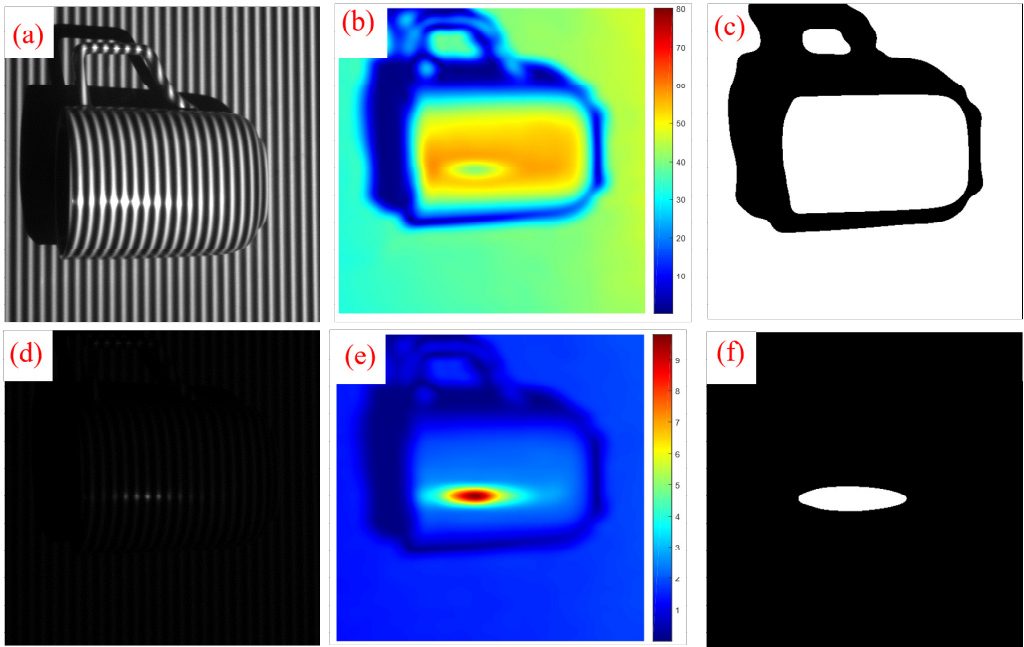
Fig. 2. Determine the saturation areas from fringes captured in different exposure times. (**a**) Normal exposure time fringe pattern; (**b**) modulation of Fig. 2**a**; (**c**) binary image of Fig. 2**b** using Otsu threshold method; (**d**) short exposure time fringe pattern; (**e**) modulation of Fig. 2**d**; (**f**) binary image of Fig. 2**e** using Otsu threshold method.

the short exposure time, respectively. Figures 2**b** and 2**e** are their modulation distribution maps. Figures 2**c** and 2**f** are the corresponding binary images of Figs. 2**b** and 2**e** by the Otsu threshold method.

3.2. Calculate the initial fringe for iteration

Our method limits the solution space of Eq. (6) by fusing a proper initial fringe as one of the inputs of the CNN denoiser. Obtaining a suitable iterative initial fringe carrying the real height information of the surface of the object for following fringe inpainting is one of the key steps of our works. As we mentioned above, the short exposure fringe has lower contrast and SNR. If the selected good quality local fringe region from the short exposure fringe is directly inserted into the corresponding saturated region of the normal exposure fringe to build the initial iterative fringe, it will result in obvious intensity difference between the filled region and the other regions in the fused fringe. In this case, it is difficult to obtain an ideal solution $\hat{x}$ of Eq. (6). In order to guarantee a satisfying result, the average value and the contrast of the local fringe selected to fill the saturated region are adjusted to close to those of the normal exposure fringe. The short exposure fringes are processed by the following three steps.

1) The intensity of the selected region from the short exposure fringe I_{dark}, used to fill the corresponding saturated region of the normal fringe I_{bright}, is adjusted in ad-

vance. First, we obtain the region Ω by dilating the selected region R. The area in Ω but outside of R is expressed as Ω/R. Second, a gray-stretched coefficient $r = \text{range}_{\text{bright}}/\text{range}_{\text{dark}}$ is calculated. The $\text{range}_{\text{dark}}$ stands for the subtraction between the minimum gray value and the average gray in the region R of the short exposure fringe pattern, and the $\text{range}_{\text{bright}}$ is calculated by subtracting the minimum gray value from the average gray in the region Ω/R of the normal exposure fringe pattern. This coefficient is used to stretch the gray level of the region R in the short exposure fringe pattern.

2) In order to obtain the fused iterative initial fringe with uniform contrast, a normalized modulation distribution $M^*(x, y)$ of the region R of the short exposure fringe pattern is calculated by the definition of $M^*(x, y) = M(x, y)/\max(M(x, y))$. Finally, for the pixels in the region R of the I_{dark}, a corrected fringe I_{dark}^* is calculated by the following equation.

$$I_{\text{dark}}^* = \frac{\text{range}_{\text{bright}}}{\text{range}_{\text{dark}}} \frac{I_{\text{dark}}}{M^*(x, y)} \tag{11}$$

3) The fused fringe pattern can be calculated by using $I_{\text{fused}} = I_{\text{dark}}^*(1 - A) + AI_{\text{bright}}$, where A is a binary matrix, in which R region is "0" and outside of R region is "1". In fact, A is the degeneration matrix corresponding to Eq. (6). I_{fused} will be used as one of the initial inputs of the iterative process of the CNN denoiser prior method. Figure 3 shows the flow chart of the fusion process.
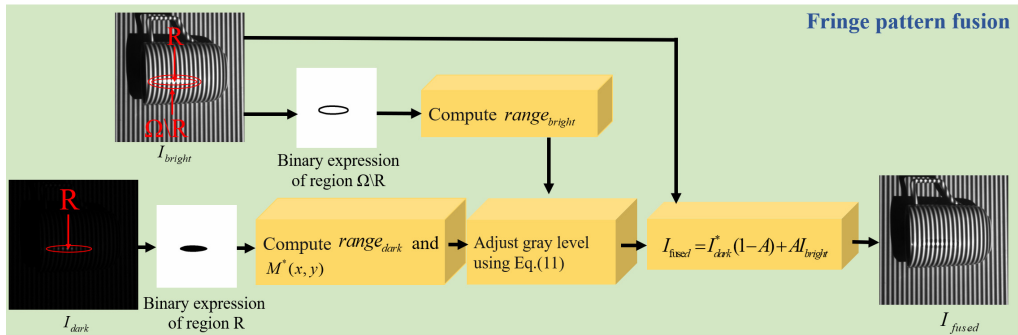

Fig. 3. Flow chart to obtain the iterative initial fringe.

3.3. Iterative inpainting process of the fringe pattern

Up to now, the image I_{fused} has been prepared. The fringe inpainting flow based on the CNN denoiser prior is shown in Fig. 4. Here the iterative initial fringe y is equal to AZ_0, where A is the degradation matrix calculated by the method in Section 3.1, and Z_0 equals I_{fused}, which is calculated by the method mentioned in Section 3.2. Taking y, A and Z_0 as the inputs of fringe inpainting system, the CNN network works for denoising. In this paper, we adopt the IRCNN [14] denoiser prior to realize fringe pattern inpainting.
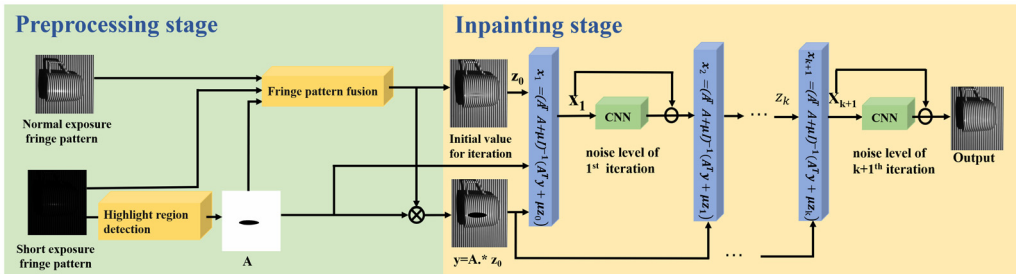
Fig. 4. Complete flow chart of the proposed fringe pattern inpainting method.

The final inpainted result will be obtained by solving the fidelity term and the regularization term with the iterative algorithm.

4. Simulation and experiment

4.1. Computer simulation

A computer simulation was carried out to verify our method. The simulated object was expressed by a two-dimensional Gaussian function. The angle between the optical axis of the camera and the optical axis of the projector optical in fringe projection
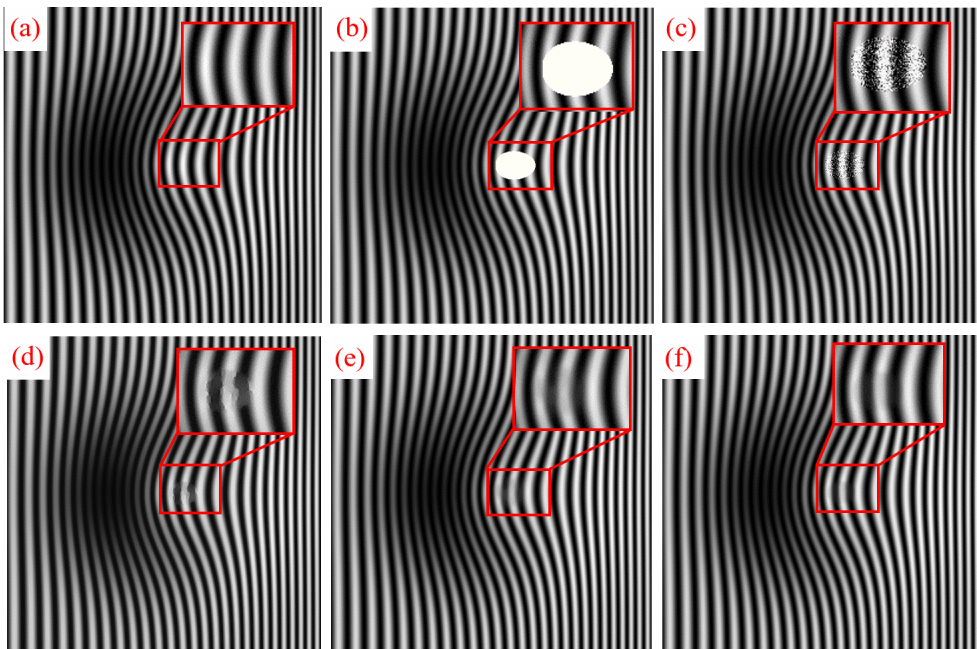
Fig. 5. Results of different inpainting methods. (**a**) Simulated fringe pattern; (**b**) simulated fringe pattern with saturated region; (**c**) the fused fringe with Gaussian noise; (**d**) inpainted result of TV-H^{-1} method; (**e**) inpainted result of the transport method; (**f**) inpainted result of the proposed method.

measurement system was set to 30°. The original fringe pattern with 512×512 pixels is shown in Fig. 5**a**. We artificially set a saturated region, where the intensity was set as "1", as shown in Fig. 5**b**. In order to simulate the procedure of the fringe inpainting, the saturated region was filled up with a sub-image, in which the intensity of each pixel is $0.9I_{bright}$ and is polluted by Gaussian noise. The fused fringe, as shown in Fig. 5**c**, is one of the inputs of the CNN denoiser. As a comparison, we compared the inpainted results of the proposed method with that of TV-H^{-1} inpainting [21] and transport inpainting [22]. The inpainted results of TV-H^{-1} inpainting algorithm and transport inpainting algorithm are shown in Figs. 5**d** and 5**e**, respectively. The inpainted result of our method is shown in Fig. 5**f**.

Since the application of the well-prepared initial fringe in the inpainting method limits the solution space of $\hat{x}$, the regularization term calculated by the CNN denoiser is effective enough. Only 5 iterations were taken to obtain the satisfied results in our method. The Table lists the comparison between the proposed method and other methods, including the number of iterations, the time consuming, the peak value of the signal-to-noise ratio (PSNR) and the root mean square error (RMSE) of the reconstructed phase from the inpainted fringe.

T a b l e. Comparison of our method, TV-H^{-1} and transport.

Methods	Iterations	Execution time	PSNR	RMSE
Initial fringe pattern	–	–	27.4880	0.4052
TV-H	100	4.61 s	31.9497	0.3050
Transport	50	75.13 s	39.9499	0.0497
Method in this paper	5	9.88 s (CPU)/**0.39 s (GPU)**	**41.6962**	**0.0440**

4.2. Experimental verification

Some experiments were carried out to verify the proposed method. The hardware system of the experiment consists of a Baumer camera with resolution of 1392×1040 pixels, a Epson projector with resolution of 1280×800 pixels and a computer. In the experiment, a cup was measured. In order to compare our method with other common methods [4, 21, 22], 25 frames of fringes corresponding to different exposure times, changing from 2000 to 50000 μs with 2000 μs increment internal, were collected. Two fringes at 50000 and 2000 μs of exposure times were used in our image inpainting method.

The proposed method is used to inpaint the fringe, and the result is compared with those of the TV-H^{-1} method [21], the transport method [22] and the multi exposure fusion method [4]. The fringes obtained by the TV-H^{-1} method, the transport method, the multi-exposure fusion method and our method are shown in Fig. 6. Figure 6**a** is the original fringe pattern. Figure 6**b** is the fused fringe, as the initial fringe for iteration in our method. Figure 6**c** is the fused pattern by the multi-exposure method [4]. Figures 6**d**–6**f** are inpainted results of the TV-H^{-1}, Transport, and CNN denoiser prior methods.
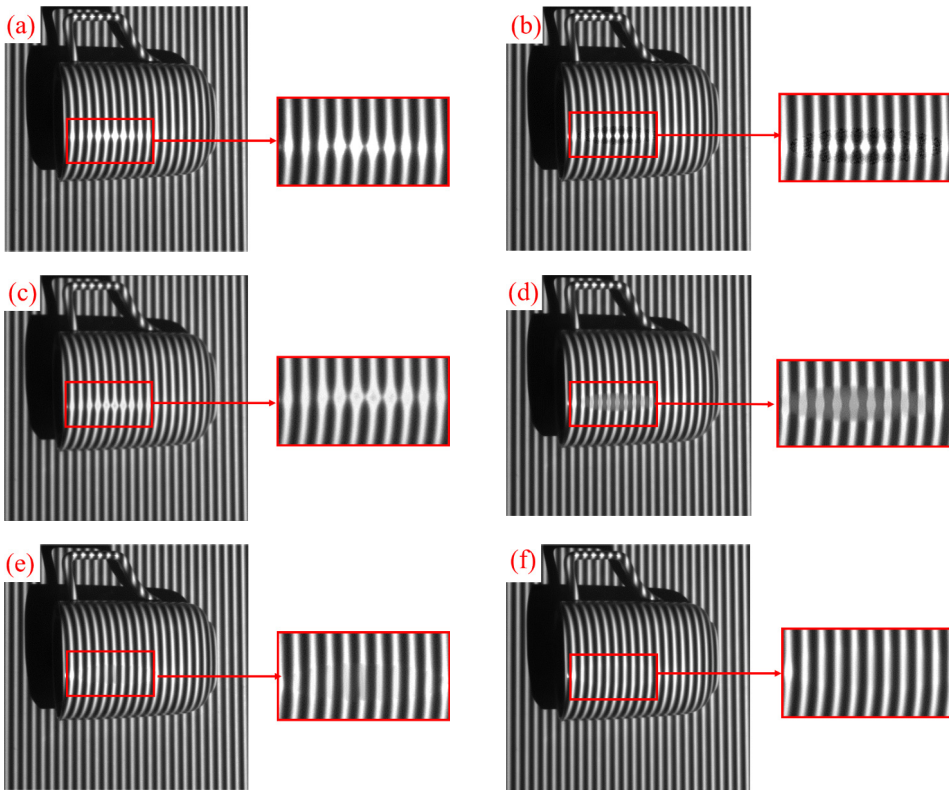
Fig. 6. Comparison of different inpainting methods. (**a**) Original fringe pattern; (**b**) fused initial fringe by our method; (**c**) fused pattern using the multi-exposure method; (**d**) inpainted result of the TV-H^{-1} method; (**e**) inpainted result of transport method; (**f**) inpainted result of the CNN denoiser prior.

We calculated the phase information from the inpainted fringes. The wrapped phase was calculated by the four-step phase shifting method. And the unwrapped phase was calculated by the modulation guided phase unwrapping algorithm [23]. Figure 7 shows the unwrapped phases distributions. Figure 7**a** is the result obtained from fringes
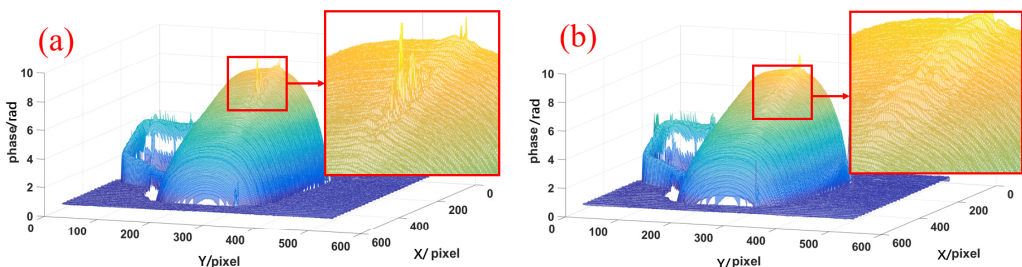
Fig. 7. Phase reconstruction of a cup. (**a**) Result of the multi-exposure method; (**b**) result of the TV-H^{-1}; (**c**) result of the transport method; (**d**) result of directly using the fused fringe; (**e**) result of the CNN denoiser prior method.
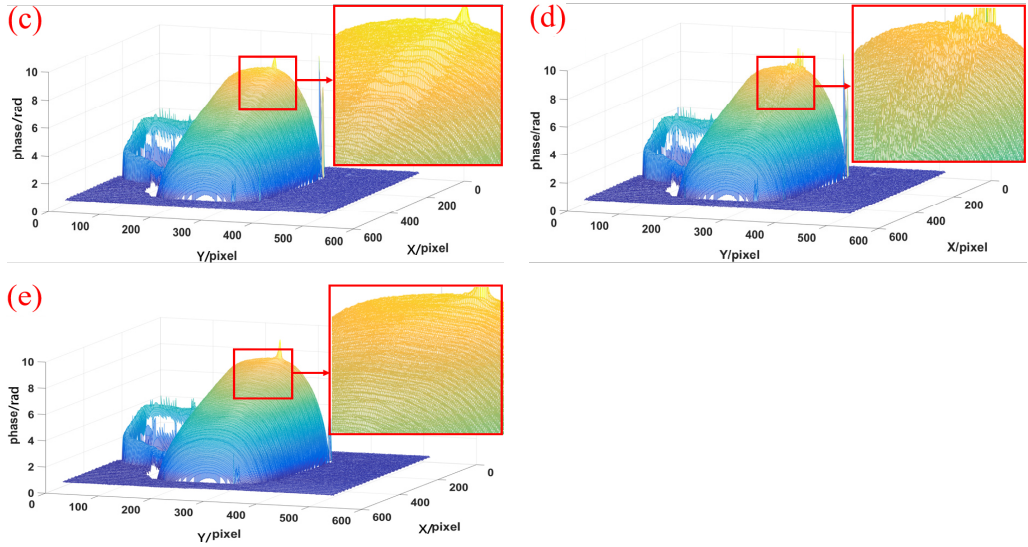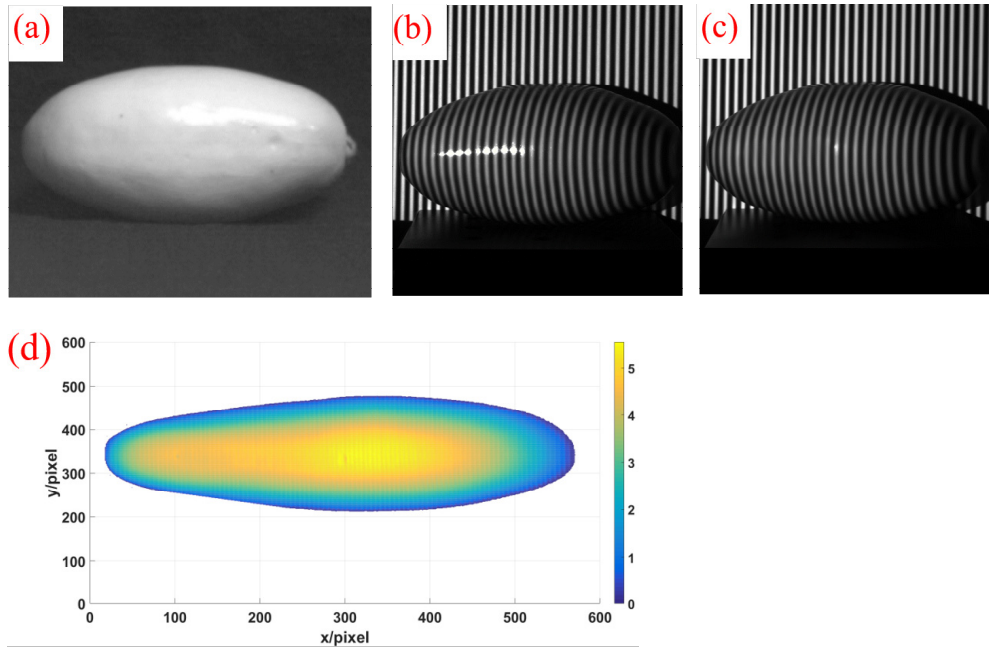
Fig. 7. Continued.

Fig. 8. Experiments for measuring plastic models. (**a**) The gray image of the plastic mango; (**b**) normal exposure fringe pattern of the mango; (**c**) inpainted fringe pattern of the mango; (**d**) reconstruction result of the mango; (**e**) the gray image of the plastic banana; (**f**) normal exposure fringe pattern of the banana; (**g**) inpainted fringe pattern of the banana; (**h**) reconstruction result of the banana.
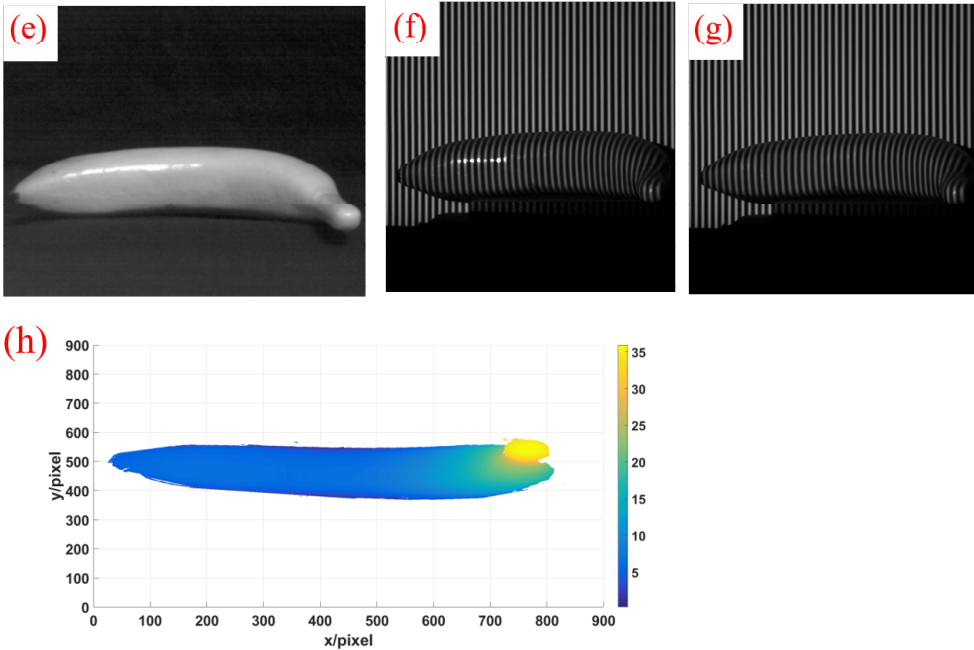
Fig. 8. Continued.

inpainted by the multi exposure fusion method. Figures 7**b**, 7**c** and 7**e** are the results obtained from the inpainted fringes by the TV-H^{-1} mehod, transport method and CNN denoiser prior method. A comparison phase map from the dual-exposure fused fringes without inpainting operation is given in Fig. 7**d**.

Other experiments have also been carried out to show that our method has a good capability. The measured objects are a plastic mango and a plastic banana, as shown in Figs. 8**a** and 8**e**. Figure 8**b** is one of the normal exposure fringe patterns of the mango, Fig. 8**c** is the inpainted fringe using the proposed method, Fig. 8**d** is the phase reconstruction result of the mango. Figure 8**f** is one of the normal exposure fringe patterns of the banana, Fig. 8**g** is the inpainted fringe pattern using the proposed method, Fig. 8**h** is the phase reconstruction result of the banana.

In the following experiment, our method is applied to reconstruct an object from fringes with a larger saturated region, as shown in Fig. 9. Figure 9**a** is a normal exposure fringe pattern, Fig. 9**b** is a short exposure fringe pattern, Fig. 9**c** is the inpainted result by our proposed method, Figs. 9**d** and 9**e** are intensity distributions of segments between 170 to 370 columns in the 256th row of the normal exposure fringe and the inpainted fringe, respectively. The reconstructed phase distribution from the fringes with saturated region and from the inpainted fringes is shown in Figs. 9**f** and 9**g**. The original image has low contrast in the saturated region, so the phase in the region is not reliable, and the phase missing region is marked in the red box.
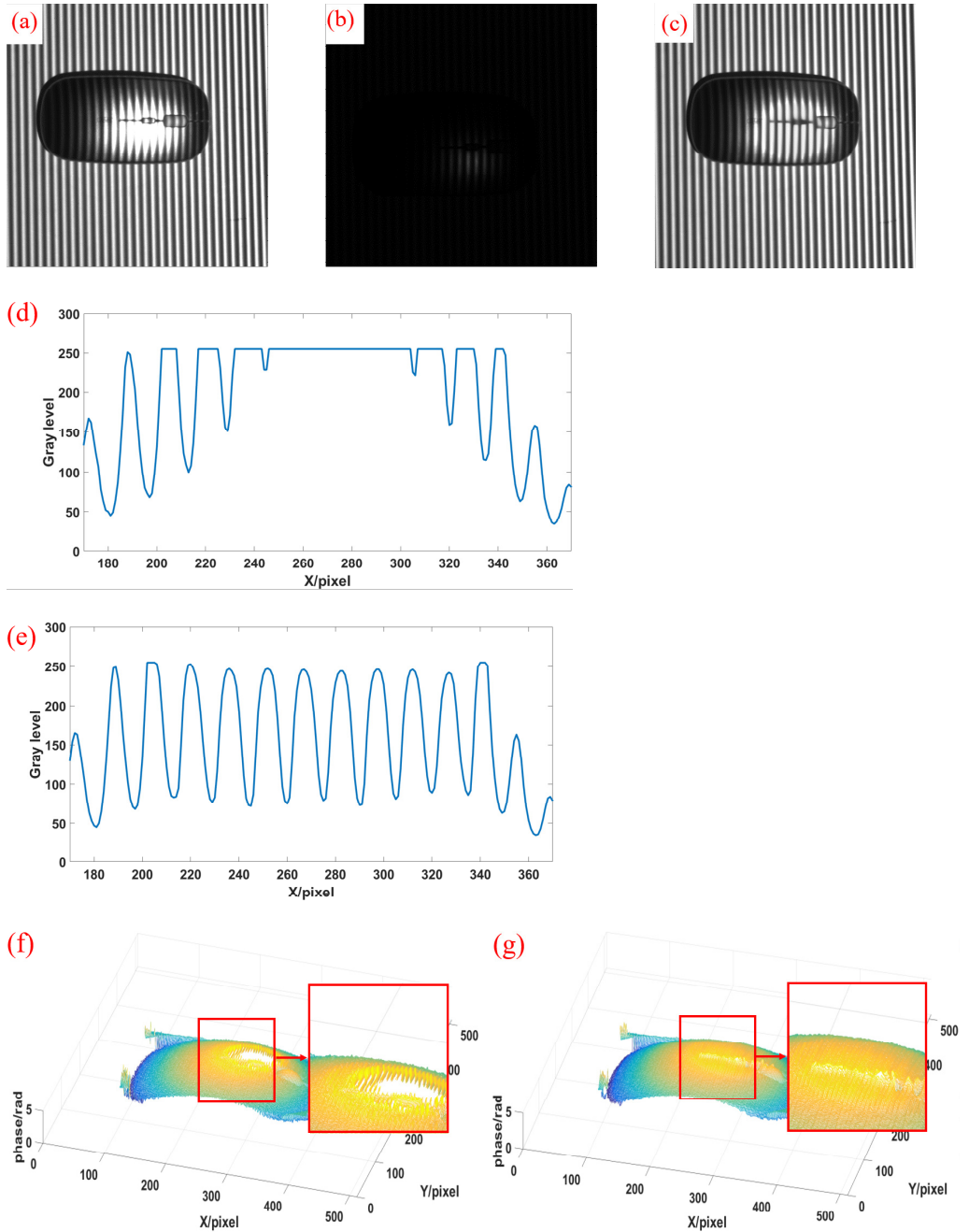
Fig. 9. Experiments for inpainting the fringe with larger saturated region. (**a**) Normal exposure fringe pattern; (**b**) short exposure fringe pattern; (**c**) inpainted result by the proposed method; (**d**) a section of intensity distribution in normal exposure fringe pattern; (**e**) a section of intensity distribution of the inpainted fringe; (**f**) reconstructed result from normal exposure fringe patterns; (**g**) reconstructed result using inpainted fringes by the proposed method.

5. Conclusion

An inpainting fringe method based on the convolutional neural network (CNN) denoiser prior using dual-exposure fringes is proposed. The modulation information of a short exposure fringe pattern is used to determine the region which needs to be inpainted. The grayscale of the short exposure fringe pattern is corrected and fused with the normal exposure fringe to form the fused fringe, as the initial fringe for the iteration. Then the high-quality fringe pattern will be obtained by the iterative inpainting method based on the CNN denoiser prior, which is used to calculate the phase corresponding to the height information on the measured object. Compared with other inpainting methods, the simulation and experimental results show that the proposed method can inpaint the fringe with saturated region quickly, even the fringe pattern with a large saturated region.

References

[1] ZUO C., CHEN Q., GU G., FENG S., FENG F., *High-speed three-dimensional profilometry for multiple objects with complex shapes*, Optics Express **20**(17), 2012, pp. 19493–19510, DOI: 10.1364/OE.20. 019493.

[2] SONG Z., CHUNG R., ZHANG X.T., *An accurate and robust strip-edge-based structured light means for shiny surface micromeasurement in 3-D*, IEEE Transactions on Industrial Electronics **60**(3), 2013, pp. 1023–1032, DOI: 10.1109/TIE.2012.2188875.

[3] SALAHIEH B., CHEN Z., RODRIGUEZ J.J., LIANG R., *Multi-polarization fringe projection imaging for high dynamic range objects*, Optics Express **22**(8), 2014, pp. 10064–10071, DOI: 10.1364/OE.22. 010064.

[4] ZHANG S., YAU S.T., *High dynamic range scanning technique*, Optical Engineering **48**(3), 2009, article 033604, DOI: 10.1117/1.3099720.

[5] LI D., KOFMAN J., *Adaptive fringe-pattern projection for image saturation avoidance in 3D surface -shape measurement*, Optics Express **22**, 2014, pp. 9887–9901, DOI: 10.1364/OE.22.009887.

[6] ZHAO H.J., LIANG X.Y., DIAO X.C., JIANG H.Z., *Rapid in-situ 3D measurement of shiny object based on fast and high dynamic range digital fringe projector*, Optics and Lasers in Engineering **54**, 2014, pp. 170–174, DOI: 10.1016/j.optlaseng.2013.08.002.

[7] BUDIANTO B., LUN D.P.K., *Inpainting for fringe projection profilometry based on iterative regularization*, 19th International Conference on Digital Signal Processing, IEEE, 2014, pp. 668–672, DOI: 10.1109/ICDSP.2014.6900748.

[8] BUDIANTO B., LUN D.P. K., *Inpainting for fringe projection profilometry based on geometrically guided iterative regularization*, IEEE Transactions on Image Processing **24**(12), 2015, pp. 5531–5542, DOI: 10.1109/TIP.2015.2481707.

[9] SHIJIE FENG, LIANG ZHANG, CHAO ZUO, TIANYANG TAO, QIAN CHEN, GUOHUA GU, *High dynamic range 3D measurements with fringe projection profilometry: a review*, Measurement Science and Technology **29**(12), 2018, article 122001, DOI: 10.1088/1361-6501/aae4fb.

[10] OTSU N., *A threshold selection method from gray-level histograms*, IEEE Transactions on Systems, Man and Cybernetics **9**(1), 1979, pp. 62–66, DOI: 10.1109/TSMC.1979.4310076.

[11] Su X.Y., Chen W.J., *Fourier transform profilometry: a review*, Optics and Lasers in Engineering **35**(5), 2001, pp. 263–284, DOI: 10.1016/S0143-8166(01)00023-9.

[12] Zuo C., Feng S.J., Huang L., Tao T.Y., Yin W., Chen Q., *Phase shifting algorithms for fringe projection profilometry: a review*, Optics and Lasers in Engineering **109**, 2018, pp. 23–59, DOI: 10.1016/j.optlaseng.2018.04.019.

[13] Su X.Y., Su L.K., Li W.S., Xiang L.Q., *A new 3D profilometry based on modulation measurement*, Proc. SPIE **3558**, Automated Optical Inspection for Industry: Theory, Technology, and Applications II, (10 August 1998), DOI: 10.1117/12.318337.

[14] Zhang K., Zuo W.M., Gu S.H., Zhang L., *Learning deep CNN denoiser prior for image restoration*, IEEE Conference on Computer Vision and Pattern Recognition, 2017, pp. 2808–2817, DOI: 10.1109/CVPR.2017.300.

[15] Zhang L., Zuo W.M., *Image restoration: from sparse and low-rank priors to deep priors* [Lecture Notes], IEEE Signal Processing Magazine **34**(5), 2017, pp. 172–179, DOI: 10.1109/MSP.2017.2717489.

[16] Zoran D., Weiss Y., *From learning models of natural image patches to whole image restoration*, IEEE International Conference on Computer Vision, 2011, pp. 479–486, DOI: 10.1109/ICCV.2011.6126278.

[17] Venkatakrishnan S.V., Bouman C.A., Wohlberg B., *Plug-and-play priors for model based reconstruction*, IEEE Global Conference on Signal and Information Processing, 2013, pp. 945–948, DOI: 10.1109/GlobalSIP.2013.6737048.

[18] Elad M., Aharon M., *Image denoising via sparse and redundant representation over learned dictionaries*, IEEE Transactions on Image Processing **15**(12), 2006, 3736–3745, DOI: 10.1109/TIP.2006.881969.

[19] Dabov K., Foi A., Katkovnik V., Egiazarian K., *Image denoising by sparse 3-D transform-domain collaborative filtering*, IEEE Transactions on Image Processing **16**(8), 2007, pp. 2080–2095, DOI: 10.1109/TIP.2007.901238.

[20] Zhang K., Zuo W.M., Chen Y.J., Meng D., Zhang L., *Beyond a Gaussian denoiser: residual learning of deep CNN for image denoising*, IEEE Transactions on Image Processing **26**(7), 2017, pp. 3142–3155, DOI: 10.1109/TIP.2017.2662206.

[21] Schönlieb C.B, Bertozzi A., *Unconditionally stable schemes for higher order inpainting*, Communications in Mathematical Sciences **9**(2), 2011, pp. 413–457.

[22] Bertalmio M., Sapiro G., Caselles V., Ballester C., *Image inpainting*, Proceedings of the 27th Annual Conference on Computer Graphics and Interactive Techniques, John Seely Brown, USA, 2000, pp. 417–424, DOI: 10.1145/344779.344972.

[23] Su X.Y., Chen W.J., *Reliability-guided phase unwrapping algorithm: a review*, Optics and Lasers in Engineering **42**(3), 2004, pp. 245–261, DOI: 10.1016/j.optlaseng.2003.11.002.